Monthly Notices
of the
ROYAL ASTRONOMICAL SOCIETY

Mon. Not. R. Astron. Soc. **404,** 1625–1632 (2010) doi:10.1111/j.1365-2966.2010.16390.x

Probing the Large Magellanic Cloud age gap at intermediate cluster masses

E. Balbinot,[1]⋆ B. X. Santiago,[1] L. O. Kerber,[2] B. Barbuy[2] and B. M. S. Dias[2]

[1]*Departamento de Astronomia, Universidade Federal do Rio Grande do Sul, Porto Alegre, RS 91501-970, Brazil*
[2]*IAG, Universidade de São Paulo, São Paulo, SP 05508-090, Brazil*

Accepted 2010 January 20. Received 2010 January 11; in original form 2009 November 12

ABSTRACT

The Large Magellanic Cloud (LMC) has a rich star cluster system spanning a wide range of ages and masses. One striking feature of the LMC cluster system is the existence of an age gap between 3 and 10 Gyr. But this feature is not clearly seen among field stars. Three LMC fields containing relatively poor and sparse clusters whose integrated colours are consistent with those of intermediate-age simple stellar populations have been imaged in *BVI* with the Optical Imager (SOI) at the Southern Telescope for Astrophysical Research (SOAR). A total of six clusters, five of them with estimated initial masses $M < 10^4\,\mathrm{M}_\odot$, were studied in these fields. Photometry was performed and colour–magnitude diagrams (CMDs) were built using standard point spread function fitting methods. The faintest stars measured reach $V \sim 23$. The CMD was cleaned from field contamination by making use of the three-dimensional colour and magnitude space available in order to select stars in excess relative to the field. A statistical CMD comparison method was developed for this purpose. The subtraction method has proven to be successful, yielding cleaned CMDs consistent with a simple stellar population. The intermediate-age candidates were found to be the oldest in our sample, with ages between 1 and 2 Gyr. The remaining clusters found in the SOAR/SOI have ages ranging from 100 to 200 Myr. Our analysis has conclusively shown that none of the relatively low-mass clusters studied by us belongs to the LMC age gap.

Key words: stars: statistics – Magellanic Clouds – galaxies: star clusters – galaxies: stellar content.

1 INTRODUCTION

The Large and Small Magellanic Clouds (LMCs and SMCs, respectively) make up a very nearby system of low-mass, gas-rich and interacting galaxies. At their distances, both Clouds can be resolved into stars, allowing their stellar populations and star formation history (SFH) to be studied in detail. These studies open up the possibility of identifying epochs of enhanced or reduced star formation and of associating them with the system dynamics (Holtzman et al. 1999; Javiel, Santiago & Kerber 2005).

Star clusters provide an alternative tool to reconstruct the SFH of a galaxy. The Magellanic Clouds have a large cluster system, spanning a wide range of properties, such as masses, ages and metallicities, which, given their proximity, can be determined using different tools (Santiago 2009). Although they make up only a small fraction of the stellar mass in a given galaxy, star clusters have an advantage over field stars in that they may be modelled as simple stellar populations (SSPs), facilitating derivation of their main properties. Sizeable samples of clusters with available integrated magnitudes and colours currently exist. In the LMC, they have been used in association with evolutionary SSP models to derive age and mass distributions and to reconstruct the initial cluster mass function and the cluster formation rate (CFR; Hunter et al. 2003; de Grijs & Anders 2006; Parmentier & de Grijs 2008).

One striking and undisputable feature of the LMC cluster system is the so-called age gap. It was proposed by Jensen, Mould & Reid (1988) as a lack of clusters in the range $4 \leq \tau \leq 10$ Gyr. Several candidates to fill this gap were proposed and discarded since then (Sarajedini 1998; Rich, Shara & Zurek 2001). Evidence for the gap is present in the CFR reconstruction by Parmentier & de Grijs (2008). An age gap is also tentatively seen in some reconstructions of the LMC SFH based on field stars, although not systematically in all fields studied and not as clearly as in the cluster system (Javiel et al. 2005; Noël et al. 2007). The lack of a clear age gap among field stars suggests that it may be less pronounced among lower mass clusters ($M < 10^4\,\mathrm{M}_\odot$) as well, which tend to be systematically disfavoured in current magnitude-limited cluster samples in the LMC. Thus, the sample of candidate clusters with well-determined

⋆E-mail: balbinot@if.ufrgs.br

ages must be pushed towards fainter limits than has been previously done.

The most reliable cluster age determinations require CMD analysis. Confrontation of observed CMDs with theoretical ones, built from stellar evolutionary models, provides the best tool for age determination of single clusters, either with the *Hubble Space Telescope* or from the ground (Piatti et al. 2007, 2009; Baume et al. 2008). Building a cluster CMD, however, is a more costly task than obtaining integrated photometry, as it requires larger telescopes with high pixel sampling and good seeing conditions. Therefore, selection of candidates to fill the LMC age gap should be based on the aforementioned samples with integrated photometry. Furthermore, poor and sparse clusters suffer from more severe field star contamination on their CMDs, something that leads to a bias towards rich LMC clusters having detailed CMD analysis available.

In this paper, we analyse the CMDs of six LMC clusters for which no CMD is yet available. Two of these clusters have integrated colours consistent with an intermediate age, according to the photometry from Hunter et al. (2003). Five of them are sparse and inconspicuous when compared to previous samples. Our main goal is to probe relatively poor and intermediate-age clusters in search of possible examples that may have ages within the age gap. They have been imaged with the Optical Imager (SOI) at the Southern Telescope for Astrophysical Research (SOAR), under $\leq$1 arcsec seeing and with excellent point spread function (PSF) sampling. In Section 2, we describe the observations and photometry. In Section 3 we present our analysis tools, including a method to efficiently decontaminate the cluster CMD from field stars. This new decontamination method uses the entire information on the magnitude and colour space to subtract field stars from the CMD. We show the results for each cluster individually. In Section 4, we present our final discussion and conclusions.

2 DATA

The observations were made in a service mode and took place on the nights of 2007 November 10 and December 16, using the SOI in *B*, *V* and *I* filters. Fields were imaged around three LMC age gap candidates listed by Hunter et al. (2003):[1] OGLE-LMC0531, KMK88-38 and OGLE-LMC0169. Another field was observed around the richer and yet unstudied cluster NGC 1878. The field around OGLE-LMC0169 was observed under unstable and mostly bad seeing for our purposes, which led us to discard the data. For the remaining fields, the mean seeing was around 0.9 arcsec during both nights.

The SOI uses two 2050 $\times$ 4100 pixel CCDs, covering a 5.26 arcmin^2 field of view (FOV) at a scale of 0.077 arcsec pixel^{-1}. The images have a gap of 10.8 arcsec between the two CCDs. A slow readout was adopted in order to minimize detector noise. A 2 $\times$ 2 binning was used, yielding a spatial scale of 0.154 arcsec pixel^{-1}.

In Table 1 we summarize the observation log, where we show the target name, filter, seeing, number of exposures and exposure time. Multiple exposures were taken in order to increase the signal-to-noise ratio (S/N) and reject cosmic rays in the final combined image. For each cluster, a set of short exposures were also taken in order to avoid saturation of bright stars. The seeing is the mean full width at half-maximum of bright stars from the individual exposures. These exposures were flat-fielded, bias-subtracted, mosaicked and combined.

[1] The names OGLE-LMC, KMK88 and BSDL refer to Pietrzynski et al. (1999), Kontizas, Metaxa & Kontizas (1988) and Bica et al. (1999), respectively.

Table 1. Log of observations.

Target	Filter	Seeing (arcsec)	Exp. time (s)
OGLE-LMC0531	*B*	0.98	3 × 600
	V	0.85	3 × 200
	I	0.81	3 × 210
	B	0.91	2 × 20
	V	0.86	2 × 15
	I	0.77	2 × 10
KMK88-38	*B*	1.01	3 × 600
	V	1.01	2 × 200
	V	1.12	2 × 200
	I	0.91	3 × 210
	B	0.86	2 × 20
	V	0.86	2 × 15
	I	0.86	2 × 10
NGC 1878	*B*	1.31	3 × 600
	V	1.15	3 × 200
	I	0.85	3 × 210
	B	1.14	2 × 20
	V	1.05	2 × 15
	I	0.91	2 × 10

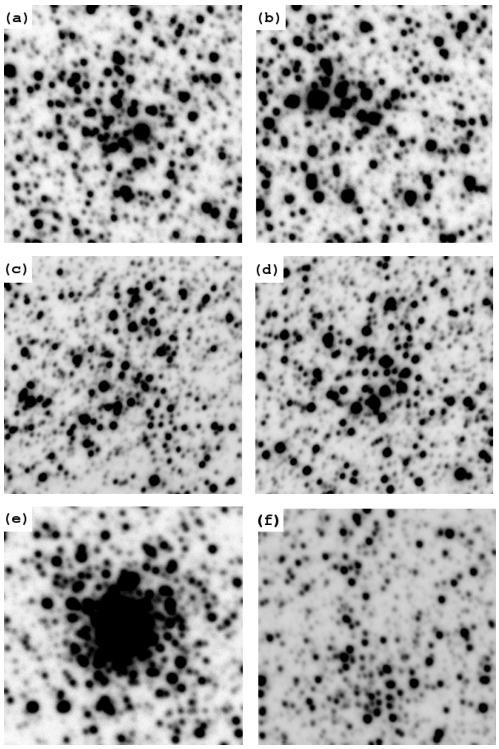

Figure 1. Sections of the final *V*-band images where the clusters are located. The size of each section is 50 $\times$ 50 arcsec^2. The cluster in each panel is as follows: (a) KMK88-38, (b) KMK88-39, (c) OGLE-LMC0531, (d) OGLE-LMC0523, (e) NGC 1878, (f) OGLE-LMC0214. In all figures, north is up and east is to the right.

The SOAR/SOI fields included three additional star clusters besides those taken from Hunter et al. (2003). They are OGLE-LMC0214, OGLE-LMC0523 and KMK88-39, respectively. The cluster names are taken from Hunter et al. (2003). Fig. 1 shows the sections (50 $\times$ 50 arcsec^2) of the final combined *V*-band images where the clusters are located. Five of them are low-density and relatively sparse open clusters; only NGC 1878 is a richer and more

compact object. To our knowledge, none of them has published CMD data in the literature.

For photometric calibration, two standard fields from Sharpee et al. (2002), located at the north-eastern arm of the SMC, were observed on each night. The observations have distinct airmasses ranging from 1.34 to 1.76. The magnitudes obtained from these images were used to fit a calibration equation for each passband (B, V and I). We took care to include standards covering a similar airmass range as the clusters and under seeing $\leq$1 arcsec. The fit residuals were $\sim$0.03 mag, indicating that both nights were photometric for most of the time.

Here we adopt a PSF fit photometry, the standard approach when dealing with crowded fields. The PSF model was computed using the images from the standard fields in order to avoid crowding effects on the PSF modelling. The photometry was carried out using DAOPHOT code from Stetson (1994). The photometry process took place as follows. (i) For each cluster, we chose the deepest and cleaner field for reference, usually the long exposure image on the I filter. Automatic detection of sources was carried out on this reference field using DAOFIND task, generating a master list of stars. (ii) This master list was then used as the position reference. (iii) The photometry on the remaining passbands then uses this master list, with only small positional offsets applied.

In Fig. 2, we show the residuals between the photometry of long and short exposures (hereafter *long* and *short*, respectively) for the cluster OGLE-LMC0531 as an example. It is clear that our photometry is accurate, since bright stars lie very near the zero residual line. Using this diagram we can determine the *long* saturation limit, where the residuals become negative. We can also determine the faint magnitude limit where the *short* S/N becomes small and the scatter in the residuals becomes larger. A systematic photometric offset of a few hundredths of magnitude was found between *short* and *long* and was interpreted as due to small seeing variations. They were dealt with by means of aperture corrections applied on the *short* magnitudes.

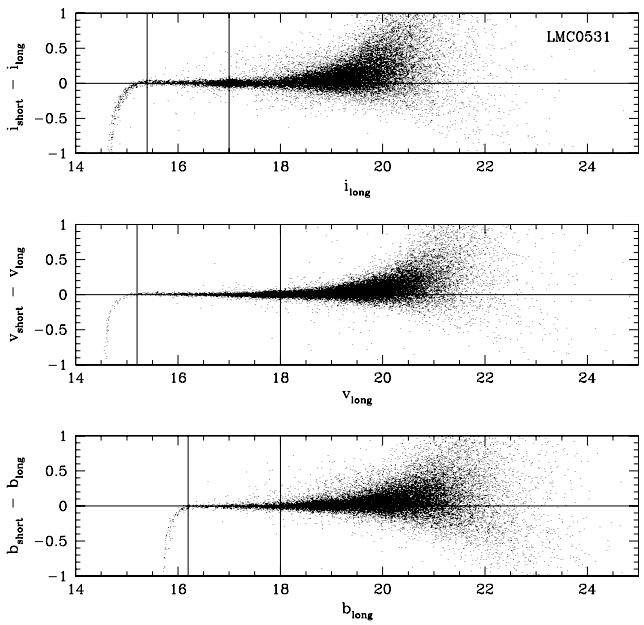

Figure 2. The residual diagrams for OGLE-LMC0531 in the B (lower panel), V (middle panel) and I (upper panel), where we show the difference between the instrumental magnitudes of the *long* and *short* images as a function of the *long* magnitude.

After photometric homogenization, we merge both *long* and *short* photometry tables. In essence, the merger process keeps only *short* stars brighter than the *long* saturation limit and only *long* stars fainter than the *short* low S/N limit. In the region between the quoted limits, we choose the star with the best magnitude measurement, i.e. the star with the smaller photometric error.

In Fig. 3, we show the result of the merging process. We also display the *long* saturation and *short* faint magnitude limits computed as previously described (solid lines). The CMDs display a characteristic shape, being dominated by the LMC fields stars, as expected, since our targets are intermediate-to-low-mass clusters. Moreover, we can distinguish the old and young population of the LMC divided by the extended Hertzsprung gap and can identify a very clear red giant branch (RGB) followed by the red clump (RC) and the asymptotic giant branch. On the blue side of the CMDs the main sequence (MS) extends to the domain of bright magnitudes, showing the presence of younger populations.

3 ANALYSIS

Since the clusters studied here are poorly populated objects, as shown in Fig. 1, it is crucial to differentiate the star cluster population from the field population. In fact, the field decontamination is the most challenging step in our analysis. For instance, KMK88-38 appears on the image as an excess of only $\sim$13 per cent relative to the same area in the field.

One popular method of decontamination is the statistical comparison of CMDs, such as the one developed by Kerber et al. (2002). In the literature, other methods are employed with success such as the statistical methods of Gallart et al. (2003), Bonatto & Bica (2007) and Piatti et al. (2008), and the proper motion analysis made by Richer et al. (2008).

3.1 Decontamination

The statistical method of Kerber et al. (2002) is based on the fact that the cluster population should appear as an overdensity in the colour–magnitude space (CMS) when compared against field stars. The decontamination is made by dividing the CMD into bins of colour and magnitude and then comparing star counts in each bin in the cluster region with the corresponding bin in the field region. This method deals with very sharp boundaries when counting stars, which leads to some shot noise when working with small numbers. The method uses a random process to select whether each star is a cluster member or not. This also leads to fluctuations on the final decontamination results.

An obvious improvement is to add an extra colour axis to the statistical field subtraction process. In this work, we explore two colours simultaneously and develop a method of decontamination that operates on the colour–colour–magnitude space (CCMS). To avoid sharp boundaries in the CCMS bins, each star is replaced by a three-dimensional Gaussian distribution with standard deviation equal to its photometric error. These additional features bring all the information available from the photometry into the analysis, using not only the position of the star in the CCMS but also its associated photometric error.

The cluster region and centre are determined by eye. Typical values for the cluster region radii are of $\sim$20 arcsec which correspond to a fraction of $\sim$1/60 of the SOAR/SOI FOV. In general, the clusters are too sparse and of low density to allow for a more systematic approach. We use all the remaining SOI area as the field region. For both the cluster and field regions, we take the following steps.

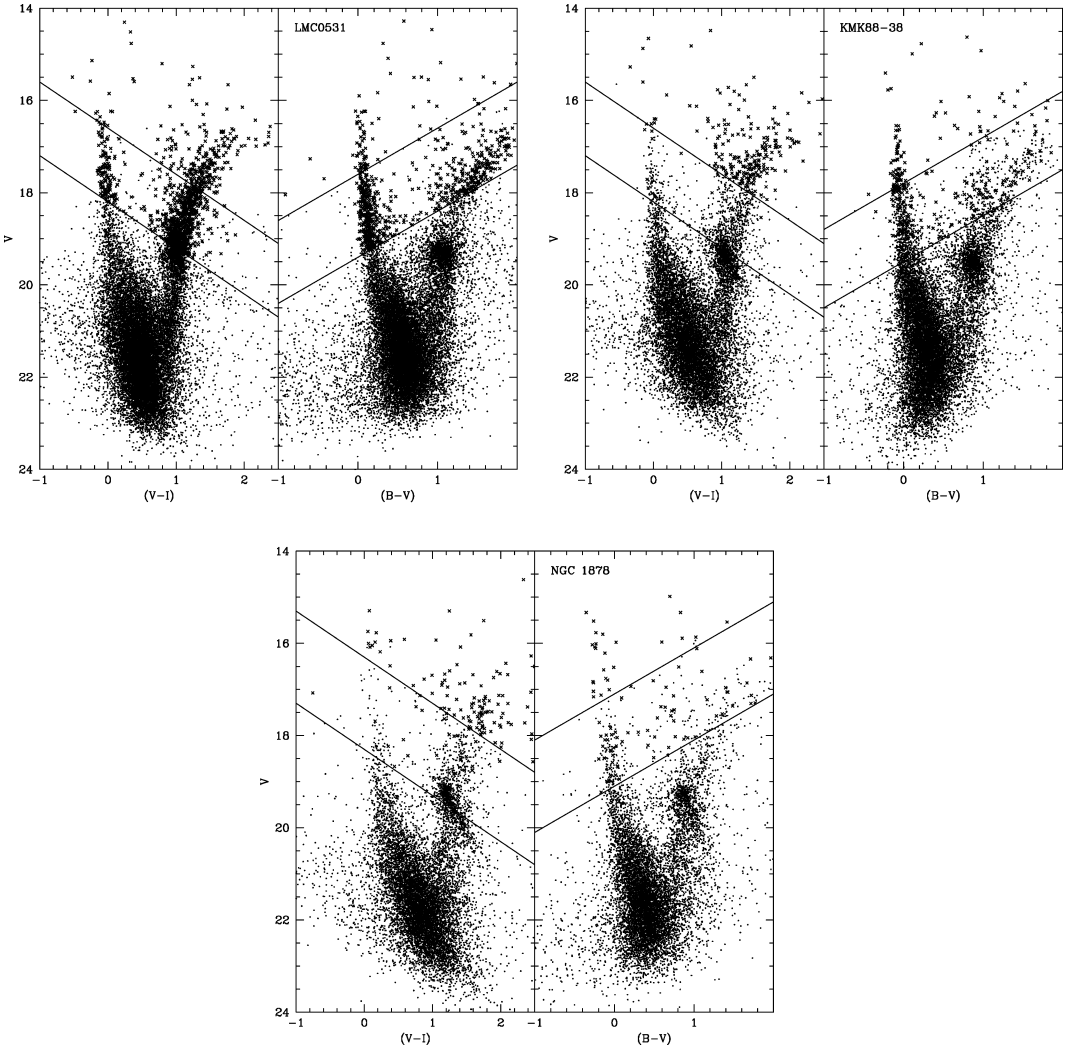

Figure 3. V, $(B-V)$ (right-hand panels) and V, $(V-I)$ (left-hand panels) CMDs from our sample. The combined *long* and *short* CMD for the entire SOI field is shown. The crosses are the stars that come from the *short* photometry and the black dots are from the *long* photometry. The upper solid line indicates the saturation limit and the lower line indicates the faint magnitude limit. The name of the cluster associated with the field is indicated in each panel.

(i) The CCMS is divided in a very fine grid of 0.01 in magnitude and 0.005 in both colours. (ii) For each bin we compute the contribution of each star by integrating its three-dimensional Gaussian over the bin volume. (iii) The resulting star counts in each bin are normalized by the different region areas.

After applying step (iii), we subtract the field star counts from the cluster ones at each bin. We then smooth out the resulting decontaminated cluster counts on CCMS by rebinning them on a coarser grid. For visualization purposes, we project the coarse CCMS grid on to the usual $(V-I)$, V and $(B-V)$, V CMD planes. The coarse grid size is chosen as the smallest possible that is able to evidence a population that resembles a SSP with minimal noise and acceptable resolution in the CMD plane. As we replaced a point process by smoothed three-dimensional Gaussians, the resulting CMDs were expressed in terms of star counts per bin.

3.2 Controlled experiments

In order to test the developed decontamination algorithm, we performed controlled experiments using artificially generated CMDs with parameters similar to those expected for the clusters in our sample.

To generate an artificial CMD, we used the aforementioned software developed by Kerber et al. (2002). This algorithm takes into account realistic photometric errors and the effects of CMD broadening due to unresolved binaries; the adopted binary fraction adopted here is 50 per cent.

We generated artificial CMDs for two isochrone models: one with log(age) = 9.1 and $Z = 0.010$ for which 50 stars were created and the other with log(age) = 8.4 and $Z = 0.010$ and containing 30 stars. 15 realizations of each model were created. Each artificial SSP realization is inserted into the real images at randomly chosen positions. By doing this we take into account effects caused by the stochastic nature of the artificial SSPs and the field.

In Fig. 4 we show the resulting decontaminated V, $(V-I)$ CMDs for the first eight of the 15 controlled experiments from the first isochrone mentioned above [log(age) = 9.1 and $Z = 0.010$, solid line]. The artificial stars generated are shown as crosses in all panels. The mean contrast relative to the field is 17 per cent. The parameters for this model are typical for the expected oldest clusters in our sample and should reflect the quality of the decontamination

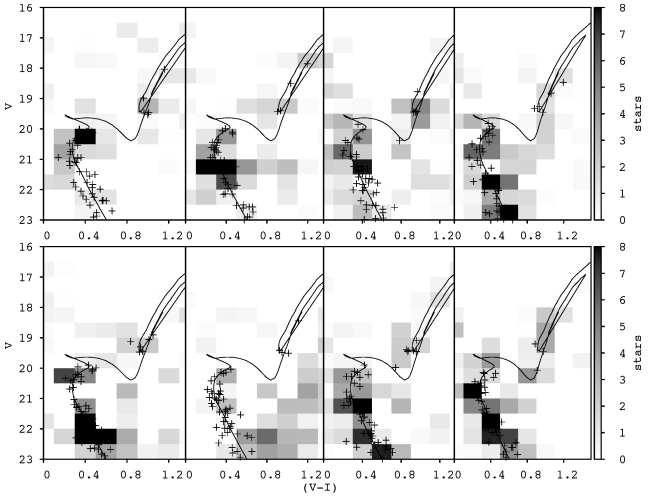

Figure 4. V, $(V - I)$ CMDs resulting from controlled experiments using an intermediate-age SSP with 50 stars. The employed isochrone is shown as the solid line in all panels. Its age is 1.25 Gyr and its metallicity is half the solar value. The artificially generated stars are shown as crosses. The field-subtracted star counts are coded with a grey-scale, which is shown as a colour bar on the right-hand side. The bin sizes in colour and magnitude are 0.2 and 0.5 mag, respectively.

algorithm for intermediate-age SSPs. We show only eight realizations of this experiment for simplicity.

Fig. 5 shows the results of the controlled experiment for the other isochrone model, with a younger age and same metallicity. The isochrone and artificial stars are again shown in all eight panels. The adopted age and metallicity [log(age) = 8.4 and $Z = 0.010$] are consistent with the youngest clusters in our sample. To test the method at yet lower contrast levels, only 30 stars were generated, yielding a mean contrast of 11 per cent.

The algorithm is successful in recovering the enhanced density contrast in the CCMS regions associated with the input SSP. Both the input MS turn-off (MSTO) and the RC positions can be identified in

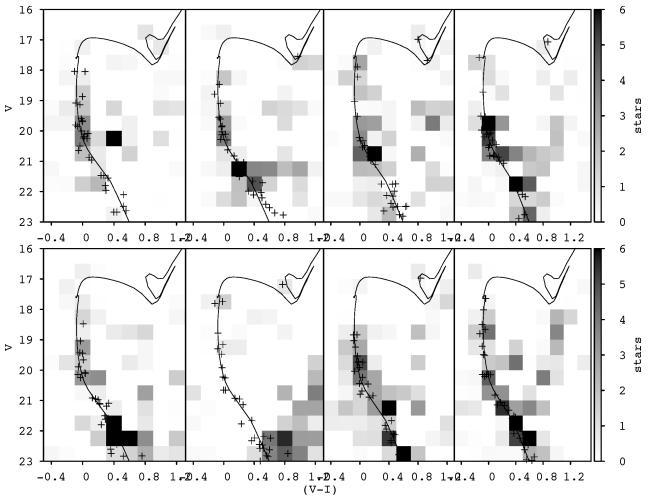

Figure 5. V, $(V - I)$ CMDs resulting from controlled experiments using a young SSP with 30 stars. The employed isochrone is shown in all panels as the solid line. It has an age of 250 Myr and a metallicity of half the solar value. The artificially generated stars are shown as crosses. The bin size and grey-scale representation of the field-subtracted star counts are the same as in the previous figure.

almost all realizations of the decontamination process applied to the first isochrone model (Fig. 4). The extended MS locus associated with the young SSP is also clearly visible in all but one of the panels of Fig. 5. The dense contaminating field and its associated fluctuations, however, often leave extra overdense CMD loci in some cases. In particular, in a couple of the realizations shown, the CMD is dominated by a faint and red plume of stars. This is likely caused by large and unaccounted photometric errors at these faint magnitudes and red colours. Considering that this plume is not associated with any reasonable SSP at the LMC distance, it can be easily discarded. More troubling is the residual field subgiant branch/RGB overdensity present in a couple of realizations shown in Fig. 5. This could make the age estimate an ambiguous task. On the other hand, addition of an extra colour, as is our case, helps us to remove this potential ambiguity. Also, in the vast majority of the realizations in both models, it is possible to identify the input SSP as the dominant excess of stars in the CMDs, on which isochrones may be visually overlaid in order to estimate their parameters.

3.3 Parameter determination

CMDs are widely used as a tool for parameter determination in the literature (Kerber, Santiago & Brocato 2007; Piatti et al. 2007), although there are alternative methods that can be employed in order to obtain similar results. These methods include integrated spectroscopy such as in Santos et al. (2006) and Ahumada et al. (2009), and integrated photometry as in Hunter et al. (2003) and Pessev et al. (2008).

Figs 6–8 show the CMDs that result from the decontamination process applied to our sample clusters. They can be used to extract physical parameters for the clusters. The target clusters are poorly populated, having typically from 20 to 150 stars. This limits the accuracy of the cluster parameter determination. Ideally, a statistical method based on CMD star counts should be used to infer ages, metallicities, distances and reddening. This has been done by several of the authors quoted in this paper. However, in the current case, we showed in the previous subsection that the fluctuation in the background field is the dominant source of noise in the decontaminated CMDs. As we cannot single out and eliminate a priori the contaminating field stars present in the cluster direction, the use of statistical methods for CMD comparison will not provide a significant advantage over isochrone fitting, as neither is capable of eliminating the effect of field contamination on the defined cluster region. This is a different situation from Balbinot et al. (2009) and Kerber et al. (2007), for instance, who used statistical CMD comparisons to infer parameters and their uncertainties for rich star clusters. Therefore, a visual isochrone fit is adequate to estimate cluster parameters in the present case. Isochrones come from the stellar evolutionary models by Girardi et al. (2002)[2].

We chose Padova isochrones although we are aware that systematic differences in the parameters may arise from the choice of one model or another. This issue has been investigated in more detail by Kerber & Santiago (2009), who compared different stellar evolution models applied to LMC clusters. They show that, in relation to Padova isochrones, the ones from BaSTI (Pietrinferni et al. 2004) tend to overestimate the age by ∼0.3 Gyr. PEL (Castellani et al. 2003) isochrones may lead to a discrepancy in the distance of ∼2.8 kpc at 50 kpc. The effects of convective overshooting (CO) are analysed in the same work. Obvious

[2] http://stev.oapd.inaf.it/cgi-bin/cmd

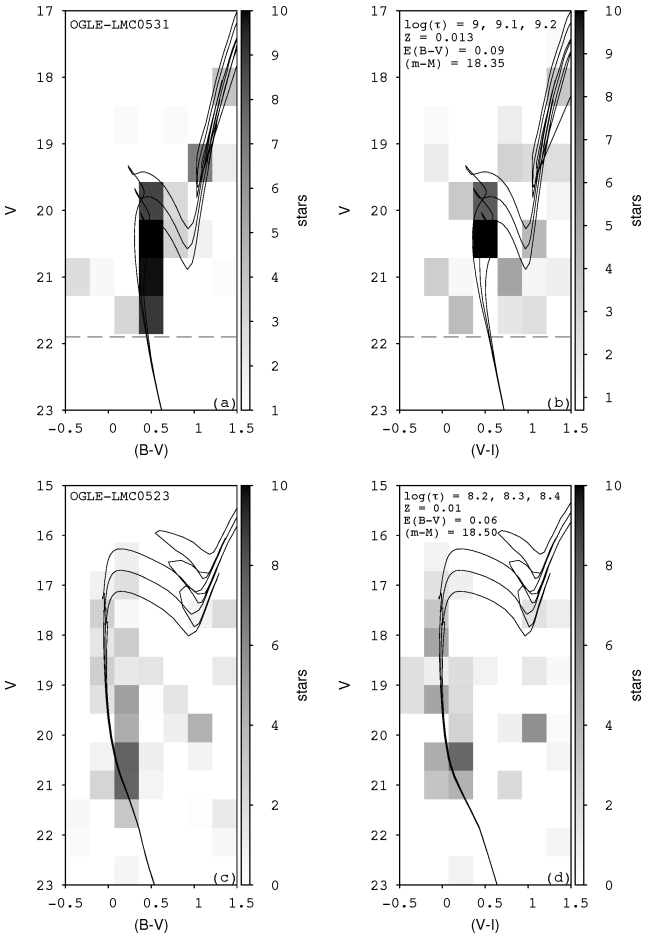

Figure 6. Panel (a): V, $(B - V)$ CMD of OGLE-LMC0531; panel (b): V, $(V - I)$ CMD for the same cluster as in the previous panel. The same model, whose isochrone parameters are indicated, was used on both CMDs. Panel (c): V, $(B - V)$ CMD of OGLE-LMC0523; panel (d): V, $(V - I)$ CMD for the same cluster as in panel (c). The same model, whose isochrone parameters are indicated, was used on both CMDs. In all panels, the field-subtracted star counts are coded with a grey-scale, which is shown as a colour bar on the right-hand side. The adopted bin size is 0.55 in magnitude and 0.30 in colour. The dashed line in the upper panels marks the position of the MSTO of a cluster with 3 Gyr and half solar metallicity.

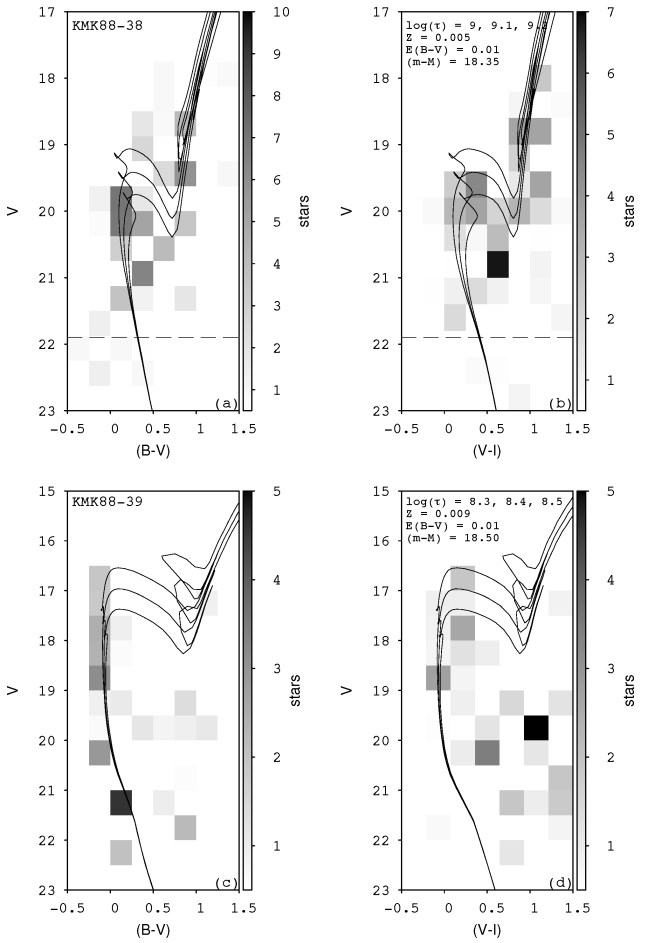

Figure 7. Same as in Fig. 6 but for the clusters KMK88-38 (panels a and b) and KMK88-39 (panels c and d). The adopted bin size is 0.40 in magnitude and 0.25 in colour.

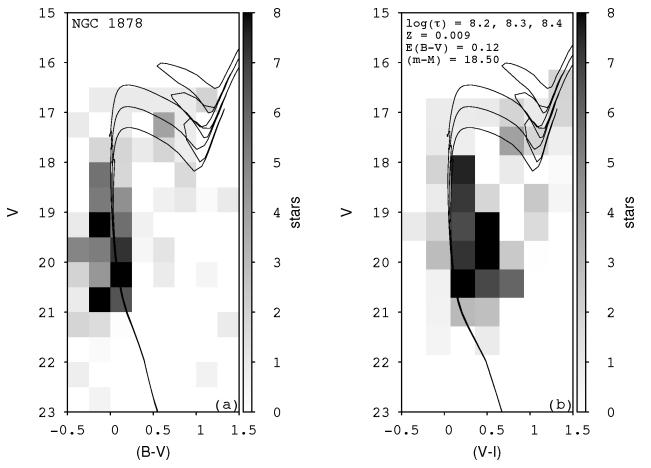

Figure 8. Same as in Fig. 6 but for the cluster NGC 1878. The adopted bin size is 0.50 in magnitude and 0.25 in colour.

differences in age arise between CO models and non-CO models, in the sense that the former yield an older age when compared to the latter [$\log(\mathrm{age})_{(\mathrm{CO})} - \log(\mathrm{age})_{(\mathrm{non-}CO)} \simeq 0.1$]. Apart from that, however, Kerber & Santiago (2009) see no other significant trend in the parameters. The authors also compared their metallicity values with those obtained from spectroscopic data (Olszewski et al. 1991; Grocholski et al. 2006) and found that the Padova models give the best agreement between spectroscopic and photometric data. We thus conclude that, for the purpose of this paper, the influence of the model adopted is negligible and the differences from model to model are much smaller than the uncertainty of our parameter determination.

For each cluster, we derive the following parameters: age, metallicity, distance and colour excess. The parameters must obey some constraints in metallicity and distance, which are typical of LMC clusters. The allowed ranges adopted here are $18.25 \leq (m - M)_0 \leq 18.75$ and $(1/3)\,\mathrm{Z}_\odot \leq Z \leq \mathrm{Z}_\odot$ (Kerber et al. 2007). We take the reddening tables from Schlegel, Finkbeiner & Davis (1998) as an initial guess of $E(B - V)$. In some cases, the lack of clear CMD structures, such as the MSTO, RGB and RC, prevents strong constraints on the parameters, specially the distance modulus. In such cases, we keep it fixed at the mean LMC value.

The results of our parameter determination are listed in Table 2. We will now comment on the results for each cluster set. In Fig. 6–8

Table 2. The result of our CMD analysis. We list the object name, the derived log(age), metallicity, $E(B-V)$ and the distance modulus. The arrows indicate upper limits. The asterisk indicates where the distance modulus was fixed at the given value.

Name	log(age)	Z	$E(B-V)$	$(m-M)_0$
OGLE-LMC0214	8.4 ↓	0.013	0.10	18.50*
OGLE-LMC0523	8.3 ↓	0.010	0.06	18.50*
OGLE-LMC0531	9.1 ± 0.1	0.013	0.09	18.35
KMK88-38	9.1 ± 0.1	0.005	0.02	18.35
KMK88-39	8.4 ↓	0.009	0.01	18.50*
NGC1878	8.3 ± 0.2	0.009	0.12	18.50*

we show, along with the subtracted CMDs, three isochrones overplotted (solid lines). All isochrones have the same metallicity and only differ by age, whose values are given in the figures. In all the figures, the V, $(B-V)$ CMD is on the left-hand side and the V, $(V-I)$ is on the right-hand side. The cluster names and other isochrone fit parameters are also shown. All CMDs show star count in bins of colour–magnitude instead of stars themselves; the grey-scale is adjusted to minimize the noise and increase the contrast for better visualization.

3.3.1 OGLE-LMC0531 and OGLE-LMC0523

These two clusters are on the same SOAR/SOI field. Only the first one is an age gap candidate. As seen in Fig. 6, the two clusters have markedly distinct ages. In fact, OGLE-LMC0531 is older, with an age between ∼1 and 2 Gyr. No sign of an upper MS is seen in either the V, $(B-V)$ or the V, $(V-I)$ CMD. In the former, its MSTO and lower MS are more clearly defined, along with a trace of its RC. As explained earlier, this allowed better constraints on its physical parameters, yielding an $E(B-V) \simeq 0.09$, $(m-M)_0 = 18.35$ and a $Z = 0.013$. The extinction value is very similar to the initial guess taken from Schlegel et al. (1998).

OGLE-LMC0523 has an age of ∼200 Myr. In reality, this is an upper limit, since no clear turn-off is seen up to the saturation limits. Since no other clear CMD structure besides the MS is detected, it was harder to constrain the cluster distance. We adopted the mean LMC distance of $(m-M)_0 = 18.50$ and found $Z = 0.010$ and $E(B-V) \sim 0.06$.

3.3.2 KMK88-38, KMK88-39 and OGLE-LMC0214

KMK88-38 is our original target in this field, as an age gap candidate. The other clusters present in the field are KMK88-39 and OGLE-LMC0214. The latter was imaged only in the V and I bands, due to variations in telescope pointing. Even though we do not show its CMDs, it has been submitted to the same analysis as the other clusters, the results of which are shown in Table 2.

The field-subtracted CMDs for KMK88-38 and KMK88-39 are shown in Fig. 7. The panels and symbol conventions are the same as in Fig. 6. KMK88-38 is relatively old, with an age between 1 and 2 Gyr, similar to OGLE-LMC0531. The presence of strong CMD features, such as an MSTO, and an RGB allowed us to explore a wider range of parameters with the effect of better constraining their determination. The derived parameters for KMK88-38 are $(m-M)_0 = 18.35$, $Z = 0.005$ and $E(B-V) = 0.02$.

On the other hand, KMK88-39 is very young, with an age of ∼250 Myr when using a metallicity of $Z = 0.009$. The age derived for this cluster is again an upper limit, since no clear MSTO is seen. The distance adopted was again the mean LMC distance, and we found a reddening of $E(B-V) = 0.01$.

3.3.3 NGC 1878

NGC 1878 was accidentally observed in place of the age gap candidate cluster BSDL917. In contrast to the other fields, only one cluster was imaged this time. Even though an NGC object, NGC 1878 had never been studied before.

Since NGC 1878 is a relatively rich cluster ($\gtrsim$100 stars), it allowed us to explore our decontamination algorithm in a simpler case, where the density of cluster stars in the CMD at a given colour–magnitude bin is significantly greater than the noise generated by the fluctuation of field stars in this same bin. In Fig. 8 we show its subtracted CMD, adopting the same panels and symbols as in the two previous figures. We clearly see much more well-defined CMD loci than in the other cases, indicating that the decontamination process is effective.

The V, $(B-V)$ CMD of NGC 1878 looks slightly bluer than expected from the V, $(V-I)$ CMD. This means that a unique isochrone solution to both CMDs was harder to achieve. As a compromise, the best visual fit solution is slightly red (blue) when compared to the main MS locus in the former (latter) CMD. This effect can result from a combination of crowding and variable PSF, which may lead to increased light contamination on PSF fitting to the B band, therefore making the star seem bluer. The best isochrone fit gives a young age, ∼200 Myr, a typical LMC metallicity of $Z = 0.009$, $E(B-V) = 0.12$. We adopted a distance modulus of $(m-M)_0 = 18.50$.

4 CONCLUSIONS

We have obtained SOAR/SOI images of three fields containing six LMC clusters, two of which were previously identified as candidates to fill the LMC age gap. Photometry was carried out in three filters (B, V and I) reaching well below the MSTO of an old stellar population.

All but one of these clusters are poor and sparse, consistent with intermediate-to-low initial masses, requiring a careful and objective process to eliminate field stars from the cluster CMD. We developed such a method that simultaneously uses the information in the available three-dimensional space of magnitudes and colours. With the resulting decontaminated CMDs, we carried out visual isochrone fits based on Padova evolutionary sequences.

Our main result is that none of the clusters studied here is older than 2 Gyr, therefore not filling the LMC age gap. The two main candidates, OGLE-LMC0531 and KMK88-38, are in fact the oldest in the sample, displaying a clear MSTO and a branch of evolved stars. Their MSTO magnitudes are about 2 mag brighter than that expected for a 3 Gyr old SSP at the LMC distance, as evidenced from Figs 6–7. Interestingly, they are sided on the images by much younger clusters, for which only upper limits in age (<200 Myr) could be derived from the CMDs. This large age range is evidence either of a complex cluster formation history or of very efficient orbital mixing within the LMC. Another noticeable result is that the ages inferred here are similar to the last two close encounters between the LMC and SMC according to recent N-body simulations (Gardiner, Sawa & Fujimoto 1994), adding a few more examples of clusters that likely have formed as the result of SMC/LMC close-by passages. We also note that the two older clusters are systematically on the foreground relative to current models for the LMC disc (Nikolaev et al. 2004; Kerber et al. 2007).

The clusters in our sample are of lower initial mass ($M \sim 10^4\,M_\odot$) than most LMC clusters studied so far. The fact that they do not fill the age gap may indicate that yet lower mass clusters, possibly cluster remnants, must be sampled and studied in order to bridge the apparent inconsistency between reconstructed cluster and field star formation histories in the LMC.

ACKNOWLEDGMENTS

This work was supported by Conselho Nacional de Desenvolvimento Científico e Tecnológico (CNPq) in Brazil and Coordenação de Aperfeiçoamento de Pessoal de Nível Superior.

REFERENCES

Ahumada A. V., Talavera M. L., Clariá J. J., Santos J. F. C., Bica E., Parisi M. C., Torres M. C., 2009, in van Loon J. T., Oliveira J. M., eds, Proc. IAU Symp. 256, The Magellanic System: Stars, Gas, and Galaxies. Kluwer, Dordrecht, p. 293
Balbinot E., Santiago B. X., Bica E., Bonatto C., 2009, MNRAS, 396, 1596
Baume G., Noël N. E. D., Costa E., Carraro G., Méndez R. A., Pedreros M. H., 2008, MNRAS, 390, 1683
Bica E. L. D., Schmitt H. R., Dutra C. M., Oliveira H. L., 1999, AJ, 117, 238
Bonatto C., Bica E., 2007, MNRAS, 377, 1301
Castellani V., Degl'Innocenti S., Marconi M., Prada Moroni P. G., Sestito P., 2003, A&A, 404, 645
de Grijs R., Anders P., 2006, MNRAS, 366, 295
Gallart C. et al., 2003, AJ, 125, 742
Gardiner L. T., Sawa T., Fujimoto M., 1994, MNRAS, 266, 567
Girardi L., Bertelli G., Bressan A., Chiosi C., Groenewegen M. A. T., Marigo P., Salasnich B., Weiss A., 2002, A&A, 391, 195
Grocholski A. J., Cole A. A., Sarajedini A., Geisler D., Smith V. V., 2006, AJ, 132, 1630
Holtzman J. A. et al., 1999, AJ, 118, 2262
Hunter D. A., Elmegreen B. G., Dupuy T. J., Mortonson M., 2003, AJ, 126, 1836
Javiel S. C., Santiago B. X., Kerber L. O., 2005, A&A, 431, 73
Jensen J., Mould J., Reid N., 1988, ApJS, 67, 77
Kerber L. O., Santiago B. X., 2009, in van Loon J. T., Oliveira J. M., eds, Proc. IAU Symp. 256, The Magellanic System: Stars, Gas, and Galaxies. Kluwer, Dordrecht, p. 391
Kerber L. O., Santiago B. X., Castro R., Valls-Gabaud D., 2002, A&A, 390, 121
Kerber L. O., Santiago B. X., Brocato E., 2007, A&A, 462, 139
Kontizas E., Metaxa M., Kontizas M., 1988, AJ, 96, 1625
Nikolaev S., Drake A. J., Keller S. C., Cook K. H., Dalal N., Griest K., Welch D. L., Kanbur S. M., 2004, ApJ, 601, 260
Noël N. E. D., Gallart C., Costa E., Méndez R. A., 2007, AJ, 133, 2037
Olszewski E. W., Schommer R. A., Suntzeff B., Harris H., 1991, AJ, 101, 515
Parmentier G., de Grijs R., 2008, MNRAS, 383, 1103
Pessev P., Goudfrooij P., Puzia T., Chandar R., 2008, AAS Meeting, 211, No. 162.27
Piatti A. E., Sarajedini A., Geisler D., Gallart C., Wischnjewsky M., 2007, MNRAS, 382, 1203
Piatti A. E., Geisler D., Sarajedini A., Gallart C., Wischnjewsky M., 2008, MNRAS, 389, 429
Piatti A. E., Geisler D., Sarajedini A., Gallart C., 2009, A&A, 501, 585
Pietrinferni A., Cassisi S., Salaris M., Castelli F., 2004, ApJ, 612, 168
Pietrzynski G., Udalski A., Kubiak M., Szymanski M., Wozniak P., Zebrun K., 1999, Acta Astron., 49, 521
Rich R. M., Shara M. M., Zurek D., 2001, AJ, 122, 842
Richer H. B. et al., 2008, AJ, 135, 2141
Santiago B. X., 2009, in van Loon J. T., Oliveira J. M., eds, Proc. IAU Symp. 256, The Magellanic System: Stars, Gas, and Galaxies. Kluwer, Dordrecht, p. 69
Santos J. F. C. Jr, Clariá J. J., Ahumada A. V., Bica E., Piatti A. E., Parisi M. C., 2006, A&A, 448, 1023
Sarajedini A., 1998, AJ, 116, 738
Schlegel D. J., Finkbeiner D. P., Davis M., 1998, ApJ, 500, 525
Sharpee B., Stark M., Pritzl B., Smith H., Silbermann N., Wilhelm R., Walker A., 2002, AJ, 123, 3216
Stetson P. B., 1994, PASP, 106, 250

This paper has been typeset from a TEX/LATEX file prepared by the author.